Effects of delay in a reaction-diffusion system under the influence of an electric field

Sumana Dutta and Deb Shankar Ray*
Indian Association for the Cultivation of Science, Jadavpur, Calcutta 700 032, India
(Received 10 September 2007; revised manuscript received 11 December 2007; published 6 March 2008)

We investigate the consequences of delay in the iodate–arsenous acid reaction under the influence of an electric field at a constant current density. Using the charge balance condition, we show how the electric field may induce an intrinsic delay in the system, which gives rise to instability. The different instability regions in the appropriate parameter space are examined. We show how the delay incites an absolute instability in a system otherwise displaying varied wave-front characteristics, viz., convective and absolute instabilities and also stationary patterns.

DOI: 10.1103/PhysRevE.77.036202 PACS number(s): 05.45.−a, 82.45.−h, 02.30.Ks, 82.20.−w

I. INTRODUCTION

The employment of ordinary partial differential equations (OPDEs) in chemical kinetics makes the obvious approximation that a reaction depends only on the current value of the variables present. At times it may happen that a phenomenon is affected by some feature of the system at an earlier time. A molecular event generally takes a small but finite amount of time to affect a molecule at some distance from it. If this process is prolonged for some reason, the delay in the system can no longer be ignored. Then delay differential equations (DDEs) become important. Such delay often materializes from feedback which is quite extensive and diverse in chemistry and biology [1,2].

DDEs have been widely employed to describe the time lag occurring between the steps of a chemical reaction as in the phosphorylation-dephosphorylation mechanism [3] and the stabilization of unstable states in illuminated thermochemical reactions [4], and in physical processes such as mass transfer across membranes [5]. Apart from these applications, DDEs have also been used to simplify the mechanisms of complicated reactions [6,7].

Keeping in mind these developments, one may envisage the presence of an external delayed feedback to gain control over reactions. Here, we attempt to study the introduction of delay in the effect of an external electric field on reaction-diffusion systems. We undertake the study by considering a general prototypical model of the iodate-iodide reductant system. This system has been widely studied for testing a variety of nonlinear dynamical features like wave-front propagation and noise-induced instabilities [8–13]. Experimental evidence of the alteration of wave-front properties of this reaction under the influence of an electric field has also been found [14,15].

In one of our previous studies [12], we have considered in detail the spatial inhomogeneities of the electric field intensity and charge density in the arsenous acid–iodate reaction. The application of the local charge balance condition, under the influence of constant current density due to ionic migration and diffusion, was shown to result in convection terms which give rise to both absolute and convective instabilities, resulting in the development of propagating waves and also stationary spatial patterns at times. It was shown that the condition of constancy of current density when maintained under a charge balance condition produces more ions [16] as a result of chemical reaction, due to stoichiometric requirements, in the presence of an externally applied field, thus generating a stronger field around the reacting zone. This process is expected to take a finite amount of time, thus resulting in an apparent change in the intensity of the local electric field, depending on the concentration of ions at some former time. Such an intrinsic lag can be expressed using the delay differential equation model. The signature of this delay in stability and wave propagation would be an interesting attribute to investigate.

In what follows, we analyze the influence of delay on the nature of spatiotemporal instability in this system and try to highlight the resulting deviations from the situation without delay. We corroborate our theoretical analysis by numerical simulations in two dimensions.

II. INTRODUCTION OF DELAY; THE MODEL

The arsenous acid–iodate reaction, one of the most common of the iodate-iodide reductant systems, is a composite of the Dushman reaction (2.1) and the Roebuck reaction (2.2):

$$IO_3^- + 5I^- + 6H^+ \rightleftharpoons 3I_2 + 3H_2O, \tag{2.1}$$

$$H_3AsO_3 + I_2 + H_2O \rightarrow H_3AsO_4 + 2I^- + 2H^+. \tag{2.2}$$

In the overall process, the Dushman reaction is the rate-determining step [8,17]. We have here followed the kinetic studies of this reaction as given by Schmitz [18], where experimental observation of the simultaneous first- and second-order dependence of the rate on $[I^-]$ over a range of low to moderately low concentration of I^- has been made. The elementary steps involved in the mechanism of the Dushman reaction as suggested by Schmitz are as follows:

$$IO_3^- + H^+ \underset{k_{-1}}{\overset{k_1}{\rightleftharpoons}} HIO_3, \tag{2.3}$$

$$HIO_3 + I^- + H^+ \underset{k_{-2}}{\overset{k_2}{\rightleftharpoons}} I_2O_2 + H_2O, \tag{2.4}$$

*pcdsr@mahendra.iacs.res.in

$$I_2O_2 + H_2O \xrightarrow{k_3} HIO_2 + HOI, \tag{2.5}$$

$$I_2O_2 + I^- \xrightarrow{k_4} IO_2^- + I_2. \tag{2.6}$$

Applying steady-state approximations to HIO_3 and I_2O_2 and considering $[H^+]$ constant (due to the large concentration of H^+ ions), and since $[H_2O]$ $(=k_w)$ is a constant, we arrive at the following rate equation:

$$\frac{d[I^-]}{dt} = -[I^-][IO_3^-][H^+]^2(k' + k''[I^-]). \tag{2.7}$$

Here, k' and k'' are constants, in keeping with the experimental rate law, and are given by

$$k' = \frac{k_1 k_2}{k_{-1}}, \tag{2.8}$$

$$k'' = \frac{k_1 k_2 k_4}{(k_{-2} + k_3) k_{-1} k_w}. \tag{2.9}$$

The experimental rate law for the system is given by

$$v = (k' + k''[I^-])[I^-][IO_3^-][H^+]^2, \tag{2.10}$$

where $k' = 4.5 \times 10^3 M^{-3}\ s^{-1}$ and $k'' = 1.0 \times 10^8 M^{-4}\ s^{-1}$ are the rate constants.

The sharp change in concentration of iodine-containing species with time makes the spatial local gradient of these species appreciably sharp, and the difference in their mobilities results in local inhomogeneity of the electric field intensity and electric charge density in the reaction medium. Furthermore, the rapidity of the reaction step, as emphasized by Münster *et al.* [19], invalidates the assumption of a homogeneous electric field. It would be relevant to consider the variation in electric potential gradient, $\nabla\phi$, by taking into consideration the charge balance condition.

The rate equations for the three ionic species $[I^-]$, $[IO_3^-]$, and $[H^+]$ are as follows:

$$\frac{d[I^-]}{dt} = -(k' + k''[I^-])[I^-][IO_3^-][H^+]^2 - \nabla \cdot \mathbf{J}_{[I^-]}, \tag{2.11}$$

$$\frac{d[IO_3^-]}{dt} = -\nabla \cdot \mathbf{J}_{[IO_3^-]}, \tag{2.12}$$

$$\frac{d[H^+]}{dt} = -\nabla \cdot \mathbf{J}_{[H^+]}, \tag{2.13}$$

where $\mathbf{J}_i$ denotes the flux of the ith ionic species for the system.

For a reaction-diffusion system, in the presence of an inhomogeneous charge density, the flux for an ionic species is given by the Nernst-Planck equation [20], viz.,

$$\mathbf{J}_i = -D_i \nabla C_i - \frac{D_i z_i F}{RT} C_i \nabla \phi, \tag{2.14}$$

where D_i denotes the diffusion coefficient, z_i is the charge on the ion i, in atomic units (with sign), and C_i is the molar concentration (mol dm^{-3}) of the ith ion. T is the absolute temperature, and R and F denote, respectively, the universal gas constant and the Faraday constant in SI units. Here, ϕ stands for the electric potential and

$$-\frac{F}{RT} \nabla \phi = \mathbf{E},$$

$\mathbf{E}$ being the electric field or the electric potential gradient in dimensions of L^{-1}. Thus, Eq. (2.14) takes the following form:

$$\mathbf{J}_i = -D_i \nabla C_i + D_i z_i C_i \mathbf{E}. \tag{2.15}$$

Now we substitute $u(x,y,t)$, $v(x,y,t)$, and $w(x,y,t)$ for $[I^-]$, $[IO_3^-]$, and $[H^+]$, respectively. Considering $D_{I^-} = D_{IO_3^-} = D_{H^+}/d = 1$, with $d=2$, we obtain the following partial differential equations (OPDEs);

$$\frac{\delta u(x,y,t)}{\delta t} = -(k' + k''u)uvw^2 + \nabla \cdot (\nabla \cdot u + u\mathbf{E}), \tag{2.16}$$

$$\frac{\delta v(x,y,t)}{\delta t} = \nabla \cdot (\nabla \cdot v + v\mathbf{E}), \tag{2.17}$$

$$\frac{\delta w(x,y,t)}{\delta t} = d\nabla \cdot (\nabla \cdot w - w\mathbf{E}). \tag{2.18}$$

Consideration of the electrical inhomogeneities of the reaction medium under the charge balance condition gives

$$\nabla \cdot \sum_i z_i \mathbf{J}_i = \mathbf{0}. \tag{2.19}$$

This implies

$$\sum_i z_i \mathbf{J}_i = \text{const} = \mathbf{j}. \tag{2.20}$$

We now put the expression for $\mathbf{J}_i$ from (2.14) into (2.21), which when rewritten in terms of the concentration of the ionic species u, v, and w gives us the expression for the electric field.

$$\mathbf{E} = \frac{\mathbf{j} - \nabla u - \nabla v + d\nabla w}{u + v + dw}. \tag{2.21}$$

Ordinary chemical kinetics has an underlying approximation that a reaction depends only on the current value of the variables present. A molecular event (at x) generally takes a small but finite amount of time [of the order of $(x-x')^2/2D$] to affect a molecule at some distance (at point x') from it [21]. This lag in the time scale can be equated to a delay time τ, given by

$$\tau \approx \frac{(x-x')^2}{2D} = \frac{(\Delta x)^2}{2D}. \tag{2.22}$$

In the present case, the ionic species under the influence of the competitive effects of the electric field and the reaction-diffusion kinetics might be considered to take a finite amount of time τ to rearrange themselves. Thus the potential field or

the local inhomogeneous electric field at any time t will depend upon the distribution of the ions at some previous time, $t-\tau$. Under such circumstances, one may write

$$\mathbf{j} = \sum_i [-D_i z_i \nabla C_i(t-\tau) + D_i z_i^2 C_i(t-\tau)\mathbf{E}(t)]. \quad (2.23)$$

Therefore the electric field in the presence of delay is given by

$$\mathbf{E}(t) = \frac{\mathbf{j} - \nabla u_{t-\tau} - \nabla v_{t-\tau} + d\nabla w_{t-\tau}}{u_{t-\tau} + v_{t-\tau} + dw_{t-\tau}}. \quad (2.24)$$

Equations (2.13)–(2.18) and (2.24) can be said to constitute the delay differential equations of the rate expressions for the system in this case.

III. LINEAR STABILITY ANALYSIS: COMPARISON BETWEEN THE OPDE AND DDE MODELS

The stability analysis for the OPDE model has already been discussed in detail in our previous paper [12]. Moreover, if the delay time is set to zero ($\tau=0$) the DDE model is equivalent to the OPDE model. So in subsequent sections we will illustrate in detail the analysis of the DDE model only.

We assume the existence of a spatially uniform steady state ($u=u_0, v=v_0, w=w_0$) of the dynamical system, such that

$$f(u_0, v_0, w_0) = 0, \quad (3.1)$$

where $f(u,v,w)$ denotes the reaction part of Eq. (2.13). We furthermore assume that this state is stable in the absence of diffusion, i.e.,

$$\left(\frac{\partial f}{\partial u}\right)_{u=u_0, v=v_0, w=w_0} = f' < 0. \quad (3.2)$$

Considering an expansion of u, v, and w in Eq. (2.13) about the steady value (u_0, v_0, w_0), we have

$$\frac{\partial(u_0+\overline{\delta u})}{\partial t} = f(u_0+\overline{\delta u}, v_0+\overline{\delta v}, w_0+\overline{\delta w}) + \nabla_{x,y}^2(u_0+\overline{\delta u}) + \nabla_x(u_0+\overline{\delta u})\left(\frac{\mathbf{j} - \nabla(u_0+\overline{\delta u}_{t-\tau}) - \nabla(v_0+\overline{\delta v}_{t-\tau}) + d\nabla(w_0+\overline{\delta w}_{t-\tau})}{(u_0+v_0+dw_0) + (\overline{\delta u}_{t-\tau} + \overline{\delta v}_{t-\tau} + d\overline{\delta w}_{t-\tau})}\right). \quad (3.3)$$

Expanding f in a Taylor series about the steady value and employing a binomial expansion for the term due to $\mathbf{E}$, while considering only the linear terms in $\overline{\delta u}$, $\overline{\delta v}$, and $\overline{\delta w}$, we have

$$\frac{\partial(\overline{\delta u})}{\partial t} = -v_0 w_0^2 k_1 \overline{\delta u} - u_0 w_0^2 k_1 \overline{\delta v} - 2u_0 v_0 w_0 k_1 \overline{\delta w} - 2u_0 v_0 w_0^2 k_2 \overline{\delta u} - u_0^2 w_0^2 k_2 \overline{\delta v} - 2u_0^2 v_0 w_0 k_2 \overline{\delta w}$$
$$+ \nabla_{x,y}^2 \overline{\delta u} - \frac{u_0 \mathbf{j}}{a_0^2}\nabla_x(\overline{\delta u}_{t-\tau} + \overline{\delta v}_{t-\tau} + d\overline{\delta w}_{t-\tau}) - \frac{u_0}{a_0}\nabla_x^2(\overline{\delta u}_{t-\tau} + \overline{\delta v}_{t-\tau} - d\overline{\delta w}_{t-\tau}) + \frac{\mathbf{j}}{a_0}\nabla_x \overline{\delta u}_{t-\tau}. \quad (3.4)$$

Here the constant sum $(u_0+v_0+dw_0)$ has been replaced by another constant a_0, for the purpose of simplicity. Proceeding similarly, Eqs. (2.17) and (2.18) take the forms

$$\frac{\partial(\overline{\delta v})}{\partial t} = \nabla_{x,y}^2 \overline{\delta v} - \frac{v_0 \mathbf{j}}{a_0^2}\nabla_x(\overline{\delta u}_{t-\tau} + \overline{\delta v}_{t-\tau} + d\overline{\delta w}_{t-\tau}) - \frac{v_0}{a_0}\nabla_x^2(\overline{\delta u}_{t-\tau}$$
$$+ \overline{\delta v}_{t-\tau} - d\overline{\delta w}_{t-\tau}) + \frac{\mathbf{j}}{a_0}\nabla_x \overline{\delta v}_{t-\tau}, \quad (3.5)$$

$$\frac{\partial(\overline{\delta w})}{\partial t} = d\nabla_{x,y}^2 \overline{\delta w} + \frac{dw_0 \mathbf{j}}{a_0^2}\nabla_x(\overline{\delta u}_{t-\tau} + \overline{\delta v}_{t-\tau} + d\overline{\delta w}_{t-\tau})$$
$$+ \frac{dw_0}{a_0}\nabla_x^2(\overline{\delta u}_{t-\tau} + \overline{\delta v}_{t-\tau} - d\overline{\delta w}_{t-\tau}) - \frac{d\mathbf{j}}{a_0}\nabla_x \overline{\delta w}_{t-\tau}. \quad (3.6)$$

We now express the spatiotemporal perturbations as

$$\overline{\delta u}(x,y,t) = Ae^{i(k_x.x+k_y.y-\omega t)}, \quad (3.7)$$

$$\overline{\delta v}(x,y,t) = Be^{i(k_x.x+k_y.y-\omega t)}, \quad (3.8)$$

$$\overline{\delta w}(x,y,t) = Ce^{i(k_x.x+k_y.y-\omega t)}, \quad (3.9)$$

where A, B, and C are constants. Substituting the above into Eqs. (3.4)–(3.6), we have

$$-i\omega A = -(v_0 w_0^2 k_1 + 2u_0 v_0 w_0^2 k_2)A - (u_0 w_0^2 k_1 + u_0^2 w_0^2 k_2)B$$
$$-2(u_0 v_0 w_0 k_1 + u_0^2 v_0 w_0 k_2)C - (k_x^2 + k_y^2)A - \frac{iu_0 \mathbf{j} k_x}{a_0^2}(A$$
$$+ B + dC)e^{i\omega\tau} + \frac{u_0 k_x^2}{a_0}(A + B - dC)e^{i\omega\tau} + \frac{i\mathbf{j}k_x}{a_0}Ae^{i\omega\tau}, \quad (3.10)$$

$$-i\omega B = -(k_x^2 + k_y^2)B - \frac{iv_0 \mathbf{j} k_x}{a_0^2}(A + B + dC)e^{i\omega\tau}$$
$$+ \frac{v_0 k_x^2}{a_0}(A + B - dC)e^{i\omega\tau} + \frac{i\mathbf{j}k_x}{a_0}Be^{i\omega\tau}, \quad (3.11)$$

$$-i\omega C = -d(k_x^2 + k_y^2)C + \frac{idw_0\mathbf{j}k_x}{a_0^2}(A + B + dC)e^{i\omega\tau}$$

$$-\frac{dw_0k_x^2}{a_0}(A + B - dC)e^{i\omega\tau} - \frac{id\mathbf{j}k_x}{a_0}Ce^{i\omega\tau}. \quad (3.12)$$

The system of Eqs. (3.10)–(3.12) can be put in the form of a matrix equation as

$$L\begin{pmatrix} A \\ B \\ C \end{pmatrix} = 0, \quad (3.13)$$

where

$$L = \begin{pmatrix} l_{11} + i\omega & l_{12} & l_{13} \\ l_{21} & l_{22} + i\omega & l_{23} \\ l_{31} & l_{32} & l_{33} + i\omega \end{pmatrix}.$$

The detailed expressions for the elements of the above matrix are given in the Appendix.

To examine the stability, we now write the following determinantal equation for the eigenvalue problem:

$$|L| = 0. \quad (3.14)$$

On expanding Eq. (3.14), we get the following dispersion relation, a cubic in ω:

$$(G_a + F_a)\omega^3 + (G_b + iF_b)\omega^2 + (G_c + iF_c)\omega + G_d + (G_e + iF_e)e^{i\omega\tau} + (G_f + iF_f)e^{2i\omega\tau} + (G_g + iF_g)e^{3i\omega\tau} + (G_h + iF_h)\omega e^{i\omega\tau} + (G_i + iF_i)\omega e^{2i\omega\tau} + (G_j + iF_j)\omega^2 e^{i\omega\tau} = 0, \quad (3.15)$$

where, G_a, G_b, G_c, etc. are the real parts and F_a, F_b, F_c, etc. are the imaginary parts of the coefficients of different powers of ω. Also $G_a=0$ and $F_a=1.0$. (For brevity, we have not mentioned the detailed expressions of the above coefficients.)

In order to obtain the variation of ω versus k_x, we find the quantity $\delta\omega/\delta k_x$ by differentiating Eq. (3.15) with respect to k_x. We then find its maxima at k_0 such that $(\delta\omega/\delta k_x)_{k_x=k_0}=0$. We thus obtain the form

$$(G_{k_0}^b + iF_{k_0}^b)\omega^2 + (G_{k_0}^c + iF_{k_0}^c)\omega + G_{k_0}^d + (G_{k_0}^e + iF_{k_0}^e)e^{i\omega\tau} + (G_{k_0}^f + iF_{k_0}^f)e^{2i\omega\tau} + (G_{k_0}^g + iF_{k_0}^g)e^{3i\omega\tau} + (G_{k_0}^h + iF_{k_0}^h)\omega e^{i\omega\tau} + (G_{k_0}^i + iF_{k_0}^i)\omega e^{2i\omega\tau} + (G_{k_0}^j + iF_{k_0}^j)\omega^2 e^{i\omega\tau} = 0, \quad (3.16)$$

where $G_{k_0}^a=(\delta G_a/\delta k_x)_{k_x=k_0}$, $G_{k_0}^b=(\delta G_b/\delta k_x)_{k_x=k_0}$, and so on. They are all implicit functions of k_x at k_0.

Only those solutions of (3.16) that satisfy the dispersion relation Eq. (3.15) are the required eigenvalues.

We now look for the parameter spaces of the constant electric flux $\mathbf{j}$ versus the wave number k_0 for which the eigenvalues exist for a fixed value of k_y. The experimentally admissible parameters [21] are given by $k'=4.5\times10^3M^{-3}\ \mathrm{s}^{-1}$, $k''=1.0\times10^8M^{-4}\ \mathrm{s}^{-1}$, and $D_{H^+}=2\times10^{-1}\ \mathrm{mm}^2\ \mathrm{s}^{-1}$ (giving $d=2$). The steady state condition used is $(u_0=2.5\times10^{-5}M,\ v_0=0.0M,\ w_0=7.1\times10^{-3}M)$.

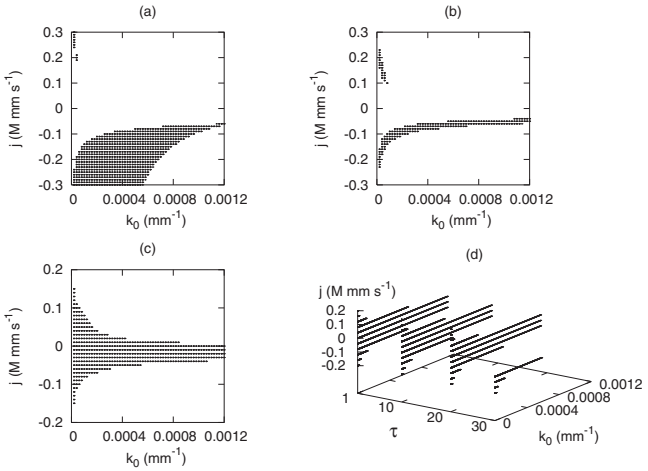

FIG. 1. The set of valid maxima of wave numbers (k_0) for each of the applied constant current density values ($\mathbf{j}$), corresponding to the eigenvalues that satisfy the condition for (a) absolute instability $\{\mathrm{Re}[\omega(k_0)]\neq0,\ \mathrm{Im}[\omega(k_0)]\neq0\}$ for $\tau=0$; (b) convective instability $\{\mathrm{Re}[\omega(k_0)]\neq0,\ \mathrm{Im}[\omega(k_0)]=0\}$ for $\tau=0$; (c) stationary pattern formation $\{\mathrm{Re}[\omega(k_0)]=0,\ \mathrm{Im}[\omega(k_0)]=0\}$ for $\tau=0$; and (d) absolute instability for $\tau=1$ to 30 (in units of Δt). (Other parameters are as mentioned in the text.)

The nature of the eigenvalues in these spaces foretells the onset of instability in the presence of both negative and positive electric flux. Following Scott and co-workers [22], we now distinguish between three typical situations; absolute instability, convective instability, and stationary pattern formation. Based on the nature of the real and imaginary parts of $\omega(k_0)$ we have

(i) $\mathrm{Re}[\omega(k_0)]\neq0$, $\mathrm{Im}[\omega(k_0)]\neq0$ (absolute instability);
(ii) $\mathrm{Re}[\omega(k_0)]\neq0$, $\mathrm{Im}[\omega(k_0)]=0$ (convective instability);
(iii) $\mathrm{Re}[\omega(k_0)]=0$, $\mathrm{Im}[\omega(k_0)]=0$ (stationary pattern formation).

Our object is to look for the set of valid maxima of the wave numbers k_0 for which the system may exhibit absolute or convective instability, or stationary pattern formation, for various values of the constant current density $\mathbf{j}$ (hereafter referred to as the $\mathbf{j}$-k_0 space). As mentioned earlier, this current density $\mathbf{j}$ can be controlled [23] from outside depending on the nature of the experiment. We discuss these cases separately in terms of the $\mathbf{j}$ versus k_0 plot in the following three paragraphs.

(1) Absolute instability. When a small perturbation lifts the system to a state different from the initial, and the perturbation moves forward, transforming the system to a final state away from the steady state, this is said to be an absolute instability. Figures 1(a) and 1(d) identify the $\mathbf{j}$-k_0 space where a small perturbation would lead to absolute instability in the system. We will return to the specific nature of the wave-front propagation under the influence of absolute instability as depicted in Fig. 2(a) in Sec. IV.

(2) Convective instability. A spatially extended system is said to be convectively unstable if a perturbation takes it away from the steady state, and propagates as a wave packet

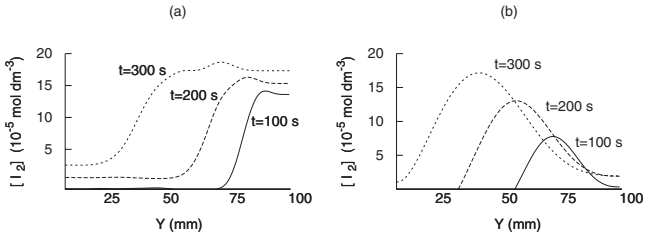

FIG. 2. Plot of the concentration of iodine versus the direction of wave propagation at different times, depicting the influence of (a) absolute instability and (b) convective instability. It can be seen that the amplitude of the wave increases with time in both cases. In the case of absolute instability the system is lifted to a state different from the initial, while in convective instability the system comes back to the initial state after the wave has passed by.

growing in size. But unlike in the case of absolute instability, in this case, when the wave packet passes by, the system comes back to the original steady state. Figure 1(b) shows the $\mathbf{j}$-k_0 space where a small perturbation would lead the system into a state of convective instability. In what follows we will again discuss the propagation of the wave front with time, when the system is convectively unstable, in Sec. IV, as portrayed in Fig. 2(b).

(3) Stationary pattern. When the perturbation is constant with time, with a purely imaginary exponent, it can give rise to a stationary pattern, i.e., the exponential part should be of the form $e^{i(k_x x+k_y y)}$, such that $\omega=0$ and k_x and k_y are real. Figure 1(c) shows the j-k_0 space for which a perturbation may bring about a transition to a pattern stationary in time.

It has been seen that for the case where $\tau=0$ (the case without delay), the system may move on to absolute or convective instability and even to a stationary pattern at times depending upon the nature of the parameter space; while in the presence of delay (nonzero τ), there exists a state of absolute instability for all values of $\mathbf{j}$. Those parameter spaces that had seen the advent of convective instability and stationary pattern formation in the absence of delay now lead to the state of absolute instability.

IV. NUMERICAL SIMULATION AND DISCUSSION

In order to make a quantitative comparison between the OPDE and DDE models, we now carry out numerical simulations of the reaction-diffusion system [Eqs. (2.13)–(2.18)] with the different expressions for the electric field [Eqs. (2.21) and (2.24), respectively], using the explicit Euler method for the integration of the equations, following discretization of space and time. A finite system size of 100 $\times$100 grid points has been chosen. Zero-flux boundary conditions have been considered along all the four walls. As for the potential, a zero-flux boundary is applied at the two sides parallel to the direction of propagation of the wave front, and a constant boundary is applied at the walls ahead of and behind the front [23], as given by

$$\nabla\phi = -\frac{\mathbf{j}}{(u_0+v_0+dw_0)}. \tag{4.1}$$

A time interval $\Delta t=1\times10^{-5}$ s and a cell size $\Delta x=0.1$ mm have been found to be appropriate for the purpose. The delay in the system can therefore be considered to be of the order of $5\Delta t$ [from Eq. (2.22)].

We have carried out our numerical simulations for both the OPDE and DDE models considering different values of $\mathbf{j}$ and τ. The initial conditions are taken identical to the initial experimental values of the reactants, with $u_0=1.0\times10^{-6}M$ and $v_0=0.006M$, over the unreacted reaction surface ahead of the front. A small area behind the front (near $Y=100$ mm) is considered as that where the reaction has already taken place; the initial value of the iodide ion here is considered to be $u_0=0.006M$, and that of the iodate $v_0=1.0\times10^{-6}M$. The hydrogen ion, or acid catalyst, that acts as a buffer is taken to be initially uniform all over the reaction vessel with a concentration of $w_0=0.0071M$. The rate constants k' and k'' are the experimentally admissible values mentioned earlier.

We calculate the iodine concentration at any time t as a function of the concentrations of iodide and iodate ions, taking into consideration the conservation of total iodine in the system:

$$[\mathrm{I}_2]_t = \frac{1}{2}([\mathrm{I}^-]_0 + [\mathrm{IO}_3^-]_0 - [\mathrm{I}^-]_t - [\mathrm{IO}_3^-]_t). \tag{4.2}$$

Figure 2 is a two-dimensional plot of the wave front as a graph of the iodine concentration versus the direction of wave propagation, at three different times. It can be seen that for the case of absolute instability [Fig. 2(a)], the wave increases in amplitude as it transforms the system from its initial state to an altogether different state. For the case of convective instability, in contrast, the amplitude of the wave increases as it moves forward, leaving the system in its original state [Fig. 2(b)].

Figure 3 depicts the wave-front characteristics, as surface plots of the iodide ion concentration, when delay is not considered in the system, for varying values of the electrical flux ($\mathbf{j}$) at long times ($t=300$ s). In the case of $\mathbf{j}=0.05M$ mm s^{-1}, convective instability is displayed, as the wave front moves forward with a maximum amplitude, and the concentration behind the wave-front decreases with time [Fig. 3(a)]. On the other hand, the reactant concentration behind the wave front may increase to a constant value, portraying absolute instability, as seen in the case of $\mathbf{j}=0.3M$ mm s^{-1} [Fig. 3(b)]. In the absence of current density $\mathbf{j}$ ($=0.0M$ mm s^{-1}), one witnesses the formation of a stationary wave [Fig. 3(c)]. Again in the case of a negative flux $\mathbf{j}=-0.1M$ mm s^{-1}, there occurs a probable culmination of a set of backward-propagating waves with high velocity [Fig. 3(d)].

In Figs. 4–7, we show surface plots of the iodide ion concentration at various times when delay ($\tau=5$, in units of Δt) is considered in the system. As the wave packet moves forward it forms a concentration gradient of the reactants, as shown in the figures. As is seen for $\mathbf{j}=0.05M$ mm s^{-1}, the system depicts absolute instability in keeping with the stability analysis (Fig. 4). Unlike in the case of the OPDE model [Fig. 3(a)], in this case the system reaches a state completely different from the initial one, once the wave has passed by [Fig. 4(d)]. Again, when $\mathbf{j}=0.3M$ mm s^{-1}, the system moves

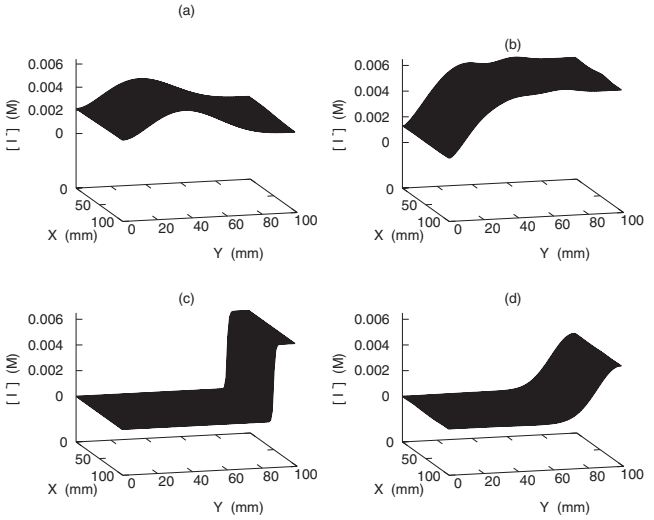

FIG. 3. Surface plots of the concentration values for the iodide ion at long time (t=300 s) in the absence of delay (τ=0) for varying current densities **j**. (a) j=0.05M mm s^{-1}, convective instability; (b) j=0.3M mm s^{-1}, absolute instability with forward-propagating wave; (c) j=0.0M mm s^{-1}, stationary wave; (d) j=−0.1M mm s^{-1}, absolute instability with backward-propagating wave. (Other parameters are as mentioned in the text.)

on to absolute instability (Fig. 5). Although the case is similar to that of the OPDE model as regards the nature of the instability, a close comparison of the final state [Fig. 5(d)] with Fig. 3(b) shows a variation in the explicit nature of the wave. Figure 6 shows the wave-front characteristics for the case when **j**=0M mm s^{-1}, where an exhibition of absolute instability may be witnessed, though the wave front is seen to be a backward-propagating one. The features of the traveling wave in the case of the negative flux (**j**=−0.1M mm s^{-1}) for the DDE model (Fig. 7) are the same

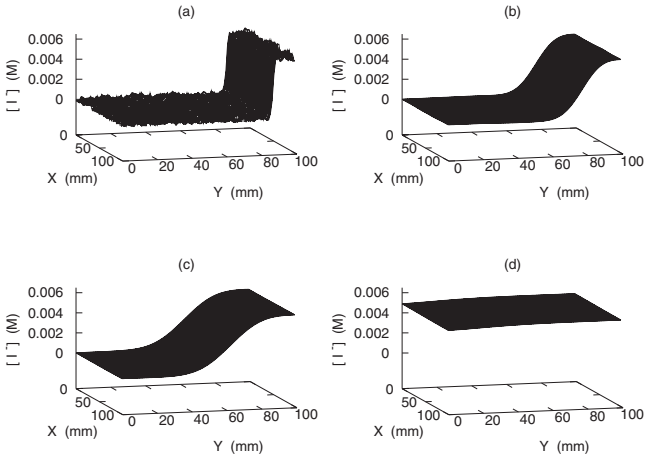

FIG. 4. Time-evolved surface plots of the concentration values for the iodide ion at a constant current density of j =0.05M mm s^{-1} showing wave propagation in the forward direction leading to absolute instability; (a) 10, (b) 100, (c) 200, and (d) 300 s, for τ=5 (in units of Δt). (Other parameters are as mentioned in the text.)

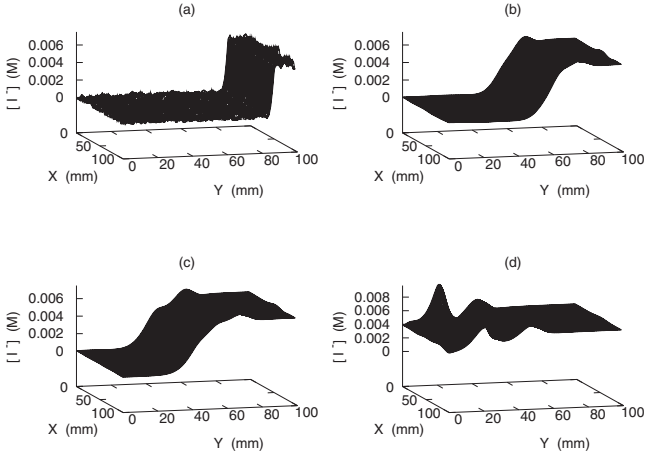

FIG. 5. Time-evolved surface plots of the concentration values for iodine at a constant current density of j=0.3M mm s^{-1} showing forward-propagating fronts and absolute instability; (a) 10, (b) 100, (c) 200, and (d) 300 s, for τ=5 (in units of Δt). (Other parameters are as mentioned in the text.)

as in the case of the OPDE model [Fig. 3(d)]. The backward-propagating wave leaves the rest of the system unreacted [Fig. 7(d)]. In keeping with our analysis, a further variation of **j** to either higher or lower values does not lead to the formation of stationary patterns nor does the system show convective instability.

The difference between the two models is also illustrated by a contour plot at four different times showing how the velocity of the wave varies in the two cases (Fig. 8). It can be seen from this figure that the inherent delay of the system gives rise to a lag in the wave-front propagation.

We also observe the time (t_m) required by the maximum of the propagating wave front to reach a particular point. This may be considered to be a measure of the propagation velocity. The initial conditions has been set as in the previous

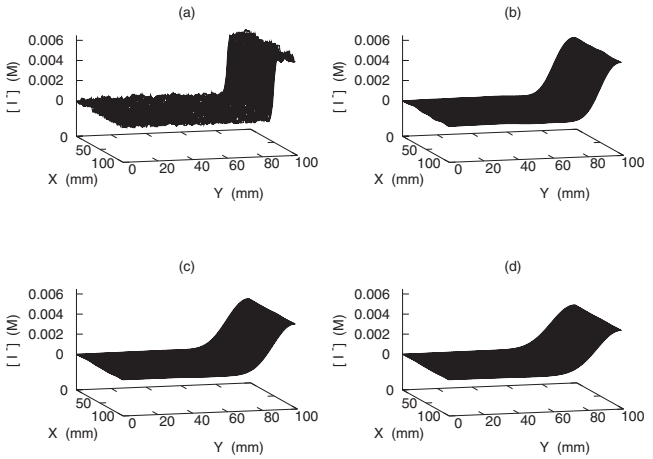

FIG. 6. Time-evolved surface plots of the concentration values for iodine in the absence of current density, j=0.0M mm s^{-1}. The plots depict backward-propagating waves of low velocity leading to absolute instability; (a) 10, (b) 100, (c) 200, and (d) 300 s, for τ =5 (in units of Δt). (Other parameters are as mentioned in the text.)

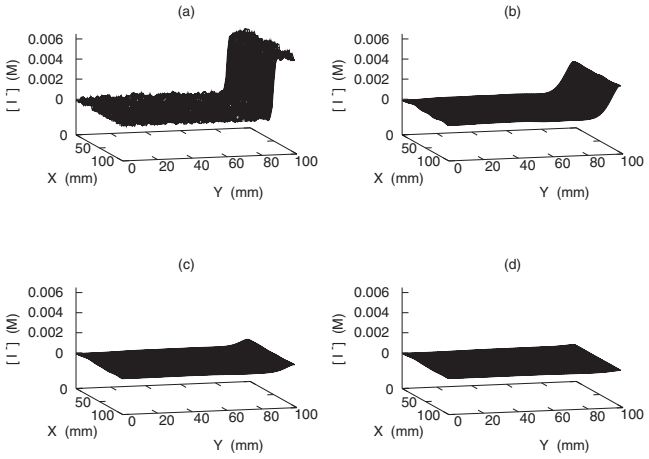

FIG. 7. Time-evolved surface plots of the concentration values for iodine at a constant current density $j=-0.1M$ mm s^{-1} showing backward-propagating waves; (a) 10, (b) 100, (c) 200, and (d) 300 s, for $\tau=5$ (in units of Δt). (Other parameters are as mentioned in the text.)

case. It is seen from a plot of t_m vs $\mathbf{j}$ (Fig. 9) that t_m varies hyperbolically with respect to $\mathbf{j}$, with asymptotes at $x=0$ and $y=0$ for $\tau=0$ and $x=0.0163$ and $y=0$ for $\tau=5$; the graphs for positive and negative $\mathbf{j}$ forming a pair of conjugate rectangular hyperbolas, with only a valid positive y axis (time axis). This gives a graphical measure of the velocity of the wave front, which changes with variation of flux $\mathbf{j}$. For the case without delay, the propagation velocity increases rapidly as $\mathbf{j}$ becomes more and more negative. While the propagation velocity is nearly zero for $\mathbf{j}=0.0M$ mm s^{-1}, it again increases as the flux moves to higher positive values. This tallies well with the analytical prediction of stationarity at zero flux. On the other hand, for the case with delay, the propagation velocity never reaches zero for $\mathbf{j}=0.0M$ mm s^{-1} or very low values of $\mathbf{j}$. The hyperbola around $\mathbf{j}=0.0163M$ mm s^{-1} is in

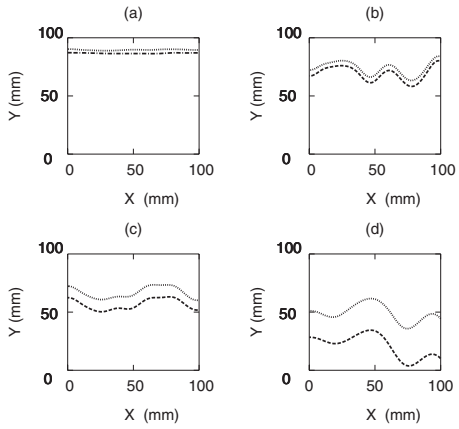

FIG. 8. Comparative time-evolved contour plots of the concentration of iodide ion for the Dushman model without (broken lines) and with delay (dotted line), having delay time $\tau=5$ (in units of Δt) and $j=0.1M$ mm s^{-1}, showing absolute instability; (a) 10, (b) 100, (c) 200, and (d) 300 s. (Other parameters are as mentioned in the text.)

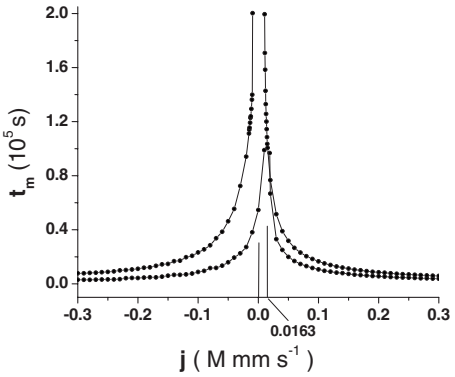

FIG. 9. Plot of t_m versus S_{T_0} for the parameter range as mentioned in the text. Solid line represents the case without delay and broken line depicts the case with delay ($\tau=5$, in units of Δt).

agreement with the analytical result that for both positive and negative values of flux the wave propagates, while for zero and very low positive flux, we observe that the system reaches absolute instability, although the velocity is small.

V. CONCLUSION

In this paper, we have studied how the delay model can be incorporated into the charge balance condition of a reaction-diffusion system under the influence of a constant external flux and how that changes the nature of the instability. It has been shown with appropriate stability analysis and corresponding numerical simulations how the presence of delay influences the propagation of the chemical wave front.

We now summarize the main conclusions of this study.

(i) We have developed an analytical approach for the inclusion of delay in the effects of electric field on a reaction-diffusion system. The analytical estimates of the threshold of instability in the iodate-iodide reductant system correspond fairly well with the numerical simulation studies.

(ii) When the presence of delay is appropriately taken care of, the system admits of absolute instability under all values of the constant current density, which is in sharp contrast to the case without delay, where, in addition to absolute instability, convective instabilities and stationary patterns were displayed by the system, depending on the value of the constant current density.

(iii) Our study indicates that the velocity of the propagating waves is controlled by the amount of flux in the system. The delay-induced effects on the reaction-diffusion system in the presence of an electric field also bring about an intrinsic lag in the velocity of the system. Since the presence of delay is almost ubiquitous in all systems under the influence of diffusion, we believe that the role played by it in inducing instability and pattern formation is generic and makes the perspective of delay-induced transition much wider.

We hope this approach will be useful for exploring delay in the selection of instability and pattern formation in spatially extended systems under the influence of an external field. The delay effects may also be externally controlled by incorporating a mechanical delay from outside, which may help us study many new interesting features of the system.

The great sensitivity of the arsenous acid–iodate reaction, which establishes it as one of the best systems for the study of wave-front propagation [17,21], also ensures the monitoring of this effect of delay, within workable ranges of experimental constants.

ACKNOWLEDGMENT

Thanks are due to the Council of Scientific and Industrial Research, Government of India, for financial support (SD).

APPENDIX

The elements of the eigenvalue matrix L are as follows:

$$l_{11} = \left(-(v_0 w_0^2 k_1 + 2u_0 v_0 w_0^2 k_2) + \frac{u_0 k_x^2}{a_0} e^{\omega\tau} - (k_x^2 + k_y^2) \right) + i\left(-\frac{u_0 j k_x}{a_0^2} + \frac{j k_x}{a_0} \right) e^{\omega\tau},$$

$$l_{12} = \left(-(u_0 w_0^2 k_1 + u_0^2 w_0^2 k_2) + \frac{u_0 k_x^2}{a_0} e^{\omega\tau} \right) + i\left(-\frac{u_0 j k_x}{a_0^2} \right) e^{\omega\tau},$$

$$l_{13} = \left(-(2u_0 v_0 w_0 k_1 + 2u_0^2 v_0 w_0 k_2) - \frac{d u_0 k_x^2}{a_0} e^{\omega\tau} \right) + i\left(-\frac{d u_0 j k_x}{a_0^2} \right) e^{\omega\tau},$$

$$l_{21} = \left(\frac{v_0 k_x^2}{a_0} \right) e^{\omega\tau} + i\left(-\frac{v_0 j k_x}{a_0^2} \right) e^{\omega\tau},$$

$$l_{22} = \left(\frac{v_0 k_x^2}{a_0} e^{\omega\tau} - (k_x^2 + k_y^2) \right) + i\left(-\frac{v_0 j k_x}{a_0^2} + \frac{j k_x}{a_0} \right) e^{\omega\tau},$$

$$l_{23} = \left(-\frac{d v_0 k_x^2}{a_0} \right) e^{\omega\tau} + i\left(-\frac{d v_0 j k_x}{a_0^2} \right) e^{\omega\tau},$$

$$l_{31} = \left(-\frac{d w_0 k_x^2}{a_0} \right) e^{\omega\tau} + i\left(\frac{d w_0 j k_x}{a_0^2} \right) e^{\omega\tau},$$

$$l_{32} = \left(-\frac{d w_0 k_x^2}{a_0} \right) e^{\omega\tau} + i\left(\frac{d w_0 j k_x}{a_0^2} \right) e^{\omega\tau},$$

$$l_{33} = \left(-\frac{d^2 w_0 k_x^2}{a_0} e^{\omega\tau} - d(k_x^2 + k_y^2) \right) + i\left(\frac{d^2 w_0 j k_x}{a_0^2} - \frac{d j k_x}{a_0} \right) e^{\omega\tau}.$$

[1] F. R. Sharpe and A. J. Lotka, Am. J. Hyg. **3** (Suppl.), 96 (1923).
[2] K. W. Smith and R. M. Noyes, J. Phys. Chem. **87**, 1520 (1983).
[3] J. Srividhya, M. S. Gopinathan, and S. Schnell, Biophys. Chem. **125**, 286 (2007).
[4] E. C. Zimmermann, M. Schell, and J. Ross, J. Chem. Phys. **81**, 1327 (1984).
[5] M. R. Roussel, J. Phys. Chem. **100**, 8323 (1996).
[6] I. R. Epstein, J. Chem. Phys. **92**, 1702 (1990).
[7] I. R. Epstein and Y. Luo, J. Chem. Phys. **95**, 244 (1991).
[8] A. Hanna, A. Saul, and K. Showalter, J. Am. Chem. Soc. **104**, 3838 (1982).
[9] D. Horváth and K. Showalter, J. Chem. Phys. **102**, 2471 (1995).
[10] J. H. Merkin and H. Ševčíková, Phys. Chem. Chem. Phys. **1**, 91 (1999).
[11] S. Dutta, S. S. Riaz, and D. S. Ray, Phys. Rev. E **71**, 036216 (2005).
[12] S. Dutta and D. S. Ray, Phys. Rev. E **73**, 026210 (2006).
[13] S. Dutta and D. S. Ray, Phys. Rev. E **75**, 066206 (2007).
[14] L. Forštová, H. Ševčíková, M. Marek, and J. H. Merkin, J. Phys. Chem. A **104**, 9136 (2000).
[15] L. Forštová, H. Ševčíková, and J. H. Merkin, Phys. Chem. Chem. Phys. **4**, 2236 (2002).
[16] H. Ševčíková and M. Marek, Physica D **9**, 140 (1983).
[17] K. Stephen Scott, *Oscillations, Waves, and Chaos in Chemical Kinetics* (Oxford University Press, New York, 1994).
[18] G. Schmitz, Phys. Chem. Chem. Phys. **2**, 4041 (2000).
[19] A. F. Münster, P. Hasal, D. Šnita, and M. Marek, Phys. Rev. E **50**, 546 (1994).
[20] J. Newman, *Electrochemical Systems* (Prentice-Hall, Englewood Cliffs, NJ, 1991).
[21] I. R. Epstein and J. A. Pojman, *An Introduction to Nonlinear Chemical Dynamics* (Oxford University Press, New York, 1998).
[22] J. R. Bamforth, S. Kalliadasis, J. H. Merkin, and S. K. Scott, Phys. Chem. Chem. Phys. **2**, 4013 (2000).
[23] Z. Virányi, Á. Tóth, and D. Horváth, Chem. Phys. Lett. **401**, 575 (2005).